Humanized mouse models to support therapeutic development for SYNGAP1 and STXBP1 disorders

Alex J. Felix[1,2,^], Brandon L. Brown[2,3,4,^], Nicolas Marotta[1,2,5], Maximilian J. Gessner[2,4], Taryn Wilson[1,2], Rani Randell[1,2], Jennine M. Dawicki-McKenna[1,2], Dulce Reinhardt[1,2], Keita Uchida[1], Michael J. Boland[2], Beverly L. Davidson[2,3,4] and Benjamin L. Prosser[1,2*].

[1]Department of Physiology, University of Pennsylvania Perelman School of Medicine, Philadelphia, PA 19104, USA.

[2]Center for Epilepsy and Neurodevelopmental Disorders (ENDD), University of Pennsylvania Perelman School of Medicine and Children's Hospital of Philadelphia, Philadelphia, PA 19104, USA.

[3]Center for Cellular and Molecular Therapeutics, Children's Hospital of Philadelphia, Philadelphia, PA 19104, USA.

[4]Department of Pathology and Laboratory Medicine, University of Pennsylvania Perelman School of Medicine, Philadelphia, PA 19104, USA.

[5]Biochemistry and Molecular Biophysics Graduate group, University of Pennsylvania Perelman School of Medicine, Philadelphia, PA 19104, USA.

^co-first authors

*to whom correspondence should be addressed:

*Benjamin L. Prosser – bpros@pennmedicine.upenn.edu

Key words: SYNGAP1, STXBP1, haploinsufficiency, epileptic encephalopathy, humanized mouse model, gene-targeted therapies.

Author emails:

Alex J. Felix: alejandro.jimenezfelix@pennmedicine.upenn.edu

Brandon L. Brown: brownb14@chop.edu

Nicolas Marotta: nick.marotta@pennmedicine.upenn.edu

Maximilian J. Gessner: gessnerm1@chop.edu

Taryn Wilson: tarynemwilson@outlook.com

Rani Randell: rrani@sas.upenn.edu

Jennine M. Dawicki-McKenna: jdawicki@pennmedicine.upenn.edu

Dulce Reinhardt: dulce.reinhardt@pennmedicine.upenn.edu

Keita Uchida: keita.uchida@pennmedicine.upenn.edu

Michael J. Boland: michael.boland@pennmedicine.upenn.edu

Beverly L. Davidson: davidsonbl@chop.edu

Acknowledgements

We thank Dr. Elizabeth A. Heller (University of Pennsylvania) for assisting with the design of the humanized mouse models and Phillip Morrin (Children's Hospital of Philadelphia) for assisting with mouse husbandry.

Funding information

This work was supported by R21 NS118280 from NIH-NINDS to B.L.P. and B.L.D., and by NDD T32 Training Grant T32NS007413 from NIH-NINDS to B.L.B.

Conflicts of interest

B.L.P. and B.L.D. are inventors on two patents relevant to therapeutic development for neurodevelopmental disorders, PCT/US2020/031672 and PCT/US2023/066948. A.J.F. and J.D.M. are inventors on PCT/US2023/066948.

Data availability statement

The data that support the findings of this study are available from the corresponding author upon reasonable request.

Author contributions

A.J.F., B.L.B., M.J.B., B.L.D and B.L.P. contributed to experimental design. A.J.F., B.L.B., T.W., R.R., M.J.G., N.M., J.D.M., D.R. performed the experiments and collected the data. B.L.B., K.U. maintained and expanded the mouse colonies. Writing original draft: A.J.F., B.L.B. Writing - Review & Editing: B.L.P., A.J.F., B.L.B, B.L.D. Funding acquisition: B.L.P, B.L.D. All authors approved the final manuscript.

Abstract

Heterozygous variants in *SYNGAP1* and *STXBP1* lead to distinct neurodevelopmental disorders caused by haploinsufficient levels of post-synaptic SYNGAP1 and pre-synaptic STXBP1, which are critical for normal synaptic function. While several gene-targeted therapeutic approaches have proven efficacious *in vitro*, these often target regions of the human gene that are not conserved in rodents, hindering the pre-clinical development of these compounds and their transition to the clinic. To overcome this limitation, here we generate and characterize *Syngap1* and *Stxbp1* humanized mouse models in which we replaced the mouse *Syngap1* and *Stxbp1* gene, respectively, with the human counterpart, including regulatory and non-coding regions. Fully humanized *Syngap1* mice present normal viability, and they were successfully crossed with a currently available *Syngap1* heterozygous knockout mouse model to generate *Syngap1* humanized-haploinsufficient mice (*Syngap1*$^{Hu/-}$). Fully humanized *Stxbp1* mice exhibit impaired viability (particularly males) and reduced STXBP1 protein abundance, precluding the generation of an *Stxbp1* humanized-haploinsufficient model. Alternatively, *Stxbp1* hybrid mice express normal levels of STXBP1 and represent a useful model to evaluate target engagement of human-specific therapeutics. *Syngap1*$^{Hu/-}$ mice display haploinsufficient levels of human SYNGAP1 and recapitulate several SYNGAP1-related phenotypes, including hyperactivity, increased repetitive behaviors, and deficits in locomotor coordination and memory. We also show that human gene-targeted antisense oligonucleotides can effectively modulate human *SYNGAP1* expression in the *Syngap1*$^{Hu/-}$ context. Overall, these humanized mouse models represent a broadly available tool to further pre-clinical therapeutic development for SYNGAP1 and STXBP1 disorders.

Introduction

De novo, heterozygous mutations in *SYNGAP1* and *STXBP1* lead to distinct, rare neurodevelopmental disorders (NDDs) with an incidence of ~1 in 10,000 and ~1 in 30,000 births, respectively (1, 2). Mutations often lead to haploinsufficient levels of post-synaptic Synaptic Ras GTPase Activating Protein 1 (SYNGAP1) and pre-synaptic Syntaxin Binding Protein 1 (STXBP1), each of which are required for proper synaptic function and neuroplasticity (3, 4). SYNGAP1 and STXBP1 epileptic encephalopathies are characterized by severe-to-profound intellectual disability, epilepsy, motor dysfunction and autistic features (5–7). No treatments currently exist that alter the course of these disorders nor that address the underlying pathomechanism.

Various *Stxbp1* heterozygous knockout mouse models (*Stxbp1*$^{+/-}$) have been generated and validated for the study of STXBP1 disorder *in vivo* (3, 8–10). *Stxbp1*$^{+/-}$ mice display haploinsufficient levels of STXBP1 protein as well as several phenotypic features associated with STXBP1 loss-of-function, including hyperactivity, impaired cognition, anxiety-like behaviors and motor dysfunction. These mouse models also recapitulate electroencephalographic (EEG) signatures observed in humans, including spike-wave discharges and myoclonic seizures (3, 9). Similarly, numerous mouse models of SYNGAP1-disease (*Syngap1*$^{+/-}$) have been developed, all of which show SYNGAP1 protein haploinsufficiency (11–13), and recapitulate clinical disease characteristics such as hyperactivity, seizures, motor impairments, and decreased spatial and working memory (11, 14). Furthermore, the initial SYNGAP1-disease model from Kim et al (12) shows alterations in EEG spectral densities that are seen clinically (15).

Several therapeutic modalities to rescue haploinsufficiency are in development for these disorders, including antisense oligonucleotide (ASO) approaches (16–18), engineered translational activators (19, 20) and CRISPR activation strategies, among others, that have proven efficacious in patient-derived induced Pluripotent Stem Cell (iPSC)-neurons. However, these candidate therapies target specific regions of the human gene that are not fully conserved in rodents, precluding *in vivo* testing in current mouse models (8, 12). This highlights the need to generate animal disease models that incorporate the molecular features of the target human gene and enable *in vivo* efficacy testing of human gene-targeted approaches, ultimately accelerating their transition to the clinic.

Towards this goal, here we generated and characterized *Syngap1* and *Stxbp1* humanized mouse models. For humanization, the entire *Syngap1* or *Stxbp1* locus from the mouse genome was excised and the respective human gene incorporated, including upstream and downstream regulatory regions, allowing broad utility for different gene-targeted strategies. Further, we generated a *Syngap1* humanized-disease mouse model that is haploinsufficient and recapitulates several SYNGAP1-disease phenotypes. We also demonstrate that human *SYNGAP1*-targeted approaches successfully modulate *SYNGAP1* expression in this model, providing an ideal platform for pre-clinical development of human-specific gene therapies.

Materials and Methods

Generation of *Syngap1* and *Stxbp1* humanized mouse models

The *Syngap1* humanized mouse model is a non-conditional knock-in (KI) model generated by introducing a ~37.5 kb of gDNA encoding the human *SYNGAP1* and *ZBTB9* genes in place of a ~34.7 kb of the murine *Syngap1* and *Zbtb9* genes (**Figure 1A**) via Bacterial Artificial Chromosome (BAC) targeting in mouse Embryonic Stem (ES) cells. The entire *Syngap1* locus is humanized (including promoter, proximal enhancers, 5'UTR, coding sequence, intronic regions and the entire 3'UTR), while the *Zbtb9* is only humanized up to the STOP codon (**Figure 1A, magenta box**). This allows for the inclusion of the *SYNGAP1* antisense transcript (*SYNGAP1-AS*) within the humanized region (**Figure 1A, orange box**), to enable testing of therapeutic approaches targeting this element. The final KI human gDNA was flanked with loxP sites. The BAC ID used for the *Syngap1* humanization is RP11-175A4. *Syngap1* humanization may affect the expression of the *Cuta* gene (**Figure 1A, brown boxes**) as *Syngap1* and *Cuta* appear to share a divergently transcribed promoter and approximately half of the region corresponding to this promoter was humanized.

The Stxbp1 humanized mouse model is a non-conditional KI model also generated by BAC targeting in mouse ES cells. The BAC replaced the murine genomic region from approximately 5.4 kb upstream of *Stxbp1* exon 1 through to near the end of exon 19 with the human genomic region from approximately 4.0 kb upstream of *STXBP1* exon 1 (Transcript ENST00000373299) through to the end of the final exon of human *STXBP1* (Transcript ENST00000636962). This represents the introduction of ~89 kb of gDNA encoding the human *STXBP1* (including promoter, proximal enhancers, 5'UTR, coding sequence, intronic regions and the entire 3'UTR) in place of ~66Kb of the murine *Stxbp1*. The final KI human gDNA was flanked with loxP sites. The humanized region may express the miR-3911 (**Figure 2A, red box**) and lncRNA ENST00000624141 (**Figure 2A, yellow box**), as well as the short 35 residue isoform of PTRH1 (Uniprot: A0A286YER0) (**Figure 2A, orange boxes**). The BAC ID used for the *Stxbp1* humanization is RP11-42D4.

All mouse gene engineering steps were performed by Ozgene. The BAC constructs for *Syngap1* and *Stxbp1* humanization were constructed by a third-party who performed quality control via restriction digestion and Pulse-Field Gel Electrophoresis. Inserted cassettes and additional modified parts of the BACs were confirmed by PCR and sequencing. Ozgene also performed independent quality controls by sequencing or qPCR of key regions such as loxP sites, neomycin and hygromycin cassettes, junctions, and presence of *SYNGAP1* and *STXBP1* transgenes. The BACs were electroporated into C57BL/6 ES cells and qPCR assays were carried out to confirm correct targeting as well as presence of the selection cassettes and the corresponding inserts. Gene-targeted ES cell clones were injected into goGermline blastocysts to produce goGermline chimeras followed by F1 heterozygous targeted mice (Hu/+) in which the selection cassettes (neomycin and hygromycin) were removed by mating the chimeras to a ubiquitous Flp line.

The resulting *Syngap1* and *Stxbp1* humanized mouse models are made available through JAX under MMRRC_069939 and MMRRC_071410, respectively.

Generation of S*yngap1* and *Stxbp1* humanized-disease mouse models

B6;129-*Syngap1*^{tm1Rlh}/J mice were obtained from The Jackson Laboratory (JAX #008890). To generate the *Syngap1* humanized-disease mouse model, male mice B6;129-Syngap1^{tm1Rlh}/J (*Syngap1*$^{+/-}$) were bred with *Syngap1*$^{Hu/Hu}$ females to generate *Syngap1*$^{Hu/-}$ and wild-type *Syngap1*$^{Hu/+}$ littermates.

B6;129S-*Stxbp1*^{tm1Sud}/J mice were obtained from The Jackson Laboratory (JAX #006381), and male mice B6;129S-*Stxbp1*^{tm1Sud}/J (*Stxbp1*$^{+/-}$) were crossed with either *Stxbp1*$^{Hu/+}$ or *Stxbp1*$^{Hu/Hu}$ females to try to generate *Stxbp1*$^{Hu/-}$ and wild-type *Stxbp1*$^{Hu/+}$ littermates.

Genotyping for B6;129-*Syngap1*^{tm1Rlh}/J and B6;129S-*Stxbp1*^{tm1Sud}/J mice was performed by Transnetyx using real-time PCR or in-house using the primer-probe sets in **Supplementary Data 1**.

Animals

The *Syngap1* humanized mouse model was maintained on a pure C57BL/6J genetic background, while B6;129-*Syngap1*^{tm1Rlh}/J mice were maintained on a mixed background of 129S1/SvImJ and C57BL/6J. The *Syngap1* humanized-disease mouse model was on a mixed background of 129S1/SvImJ and C57BL/6J. The *Stxbp1* humanized model was maintained on a mixed genetic background of C57BL/6J outcrossed one generation to the BALB/c strain. B6;129S-*Stxbp1*^{tm1Sud}/J mice were maintained in a pure C57BL/6J background. *Stxbp1* humanized-disease mice were on a mixed background of C57BL/6J and BALB/c strain.

Both male and female mice were used in this study. Animals were housed at the University of Pennsylvania Perelman School of Medicine animal facility or at the Children's Hospital of Philadelphia (CHOP) in accordance with the standards set forth by the University of Pennsylvania Institutional Animal Care and Use Committee or CHOP's Institutional Animal Care and Use Committee and the Guide for the Care and Use of Laboratory Animals published by the US National Institutes of Health under protocol #807524. Mice were maintained on a 12:12-h light:dark cycle with *ad libitum* access to food and water and were weaned at 21 days. For *Syngap1* and *Stxbp1* humanized mouse models, body weight measurements were obtained twice per week until animals reached 12 weeks of age. For the *Syngap1* humanized-disease mouse model, body weights were recorded weekly until mice reached 15 weeks of age. Survivability was assessed up to 36 weeks of age.

Both male and female mice were generated at CHOP for behavioral phenotyping. Genetic background of these mice (*Syngap1*$^{Hu/-}$ and *Syngap1*$^{Hu/+}$) were confirmed by miniMUGA testing of 1 mouse per litter and showed a genetic background of ~85% C57BL/6J.

Copy number variation assay

Ear samples or tail snips from mice were collected in 1.5 mL tubes for genotyping. Genomic DNA (gDNA) extraction was performed by adding 100 µL of DirectPCR Lysis Reagent (Viagen Biotech #402-E) supplemented with proteinase K (Viagen Biotech #505-PKP) and incubating the samples at 56 °C overnight. Proteinase K was then inactivated at 86 °C for 45 min and samples were centrifuged at 8,000 x g for 1 min. The supernatant containing gDNA was directly used for qPCR-based genotyping or stored at 4 °C.

The copy number variation assay with qPCR was prepared by mixing the following reagents: 1 µL of crude gDNA, 1X PrimeTime Gene Expression Master Mix (IDT #1055772), 1X primers/probe mix and nuclease-free water to a final volume of 10 µL. Three technical replicates were performed for each sample. qPCR was carried out on a QuantStudio 3 Real-Time PCR System (ThermoFisher) with a passive reference of ROX using the following cycling conditions: 95 ºC for 3 min for 1 cycle, 95 ºC for 15 s and 62 ºC for 1 min for 40 cycles. ΔCt was calculated by subtracting the average Ct of the reference gene from the average Ct of the gene of interest for each sample. ΔΔCt values were obtained by subtracting the average ΔCt value of the control sample from the ΔCt of the test samples and then converted into $2^{-\Delta\Delta Ct}$ to obtain the fold change of gene expression. Mouse *Tert* was used as endogenous control. In all reactions, samples from WT animals (+/+) were included to determine a reference Ct value corresponding to the presence of two copies of the mouse allele.

RNA isolation and RT-qPCR

Isolated brain tissue (~1/4 of a cortex for *Stxbp1* and *Syngap1* humanized mouse models or hemi-brain for *Syngap1* humanized-disease mice) was mixed with 1 mL of TRIzol reagent (Invitrogen #15596018) and a 5 mm stainless steel bead (Qiagen #69989) in an RNase-free microcentrifuge tube. Brain tissue was then homogenized in a TissueLyser LT homogenizer (Qiagen #85600) for 5 min at 50 Hz. The homogenate was centrifuge at 12,000 x g for 5 min at 4 °C and seated for an additional 5 min to precipitate insoluble debris. The supernatant was transferred to a new tube, mixed with 200 µL of chloroform (Acros Organics #190764), shaken vigorously and centrifuged at 12,000 x g for 15 min at 4 °C. Aqueous phase was transferred to a new tube containing 500 µL of ice-cold isopropanol (Sigma-

Aldrich #190764) followed by incubation for 10 min on ice and centrifugation at 12,000 x g for 10 min at 4 °C to precipitate RNA. Supernatant was discarded and 1 mL of ice-cold 75% ethanol (Decon laboratories #2701) was added to wash the pellet followed by centrifugation at 7,500 x g for 5 min at 4 °C. Supernatant was again discarded and RNA pellet was air-dried for 20 min. RNA was resuspended in 100 µL of RNase-free water and allowed to reconstitute for 10 min at 56 °C. To ensure RNA integrity for downstream applications, the resuspended RNA was purified using the Quick RNA Miniprep kit (Zymo #R1055) following manufacturer's instructions. Purified RNA was resuspended in 50 µL of RNase-free water. RNA concentration was determined by measuring OD_{260} nm absorbance in a Synergy HTX reader (Biotek).

cDNA synthesis was performed using the SuperScript IV First-Strand Synthesis System with ezDNase Enzyme (ThermoScientific #18091300) using random hexamer primers according to manufacturer's instructions. The ezDNase treatment step was performed for all conditions.

Probe-based qPCR was prepared by mixing the following reagents: 1 µL of cDNA, 1X PrimeTime Gene Expression Master Mix (IDT #1055772), 1X primers/probe mix and nuclease-free water to a final volume of 10 µL. Three technical replicates were performed for each sample. qPCR was carried out on a QuantStudio 3 Real-Time PCR System (ThermoFisher) with a passive reference of ROX using the following cycling conditions: 95 ºC for 3 min for 1 cycle, 95 ºC for 5 s and 60 ºC for 30 s for 40 cycles. ΔCt was calculated by subtracting the average Ct of the reference gene from the average Ct of the gene of interest for each sample. ΔΔCt values were obtained by subtracting the average ΔCt value of control samples from the ΔCt of the test samples and then converted into $2^{-\Delta\Delta Ct}$ to obtain the fold change of gene expression.

All qPCR primer probe sets sequences can be found in **Supplementary Data 1**.

Protein isolation and Western blot

For characterization of the *Syngap1* and *Stxbp1* humanized mouse models, isolated cortices (~1/4 of cortex per animal) were mixed with 500 µL of 1.5x Laemmli buffer [15% glycerol (Amresco #M152), 3% SDS (Sigma #L5750), 3.75 mM EDTA (Bio-Rad #1610729) and 75 mM Tris, pH 7.5 (Invitrogen #15567027)] in a 2 mL sample tube (Qiagen #990381), and a 5 mm stainless steel bead (Qiagen #69989) was added. Tissue was then homogenized in a TissueLyser LT homogenizer (Qiagen #85600) for 5 min at 50 Hz followed by incubation at 95 ºC during 10 min. Protein lysates were briefly spun down and the supernatants were transferred to a new microcentrifuge tube. For characterization of the *Syngap1* humanized-disease mouse model, hemi-brains were mixed with 750 µL of 1X RIPA buffer (Cell Signaling Technology #9806S) supplemented with phosphatase (PhosSTOP, Roche #4906845001) and protease (cOmplete, Roche #11836170001) inhibitor cocktails and homogenized as described above.

Protein extracts were quantified using the Pierce 660nm Protein Assay Kit (Thermo #22662) supplemented with Ionic Detergent Compatibility Reagent (Thermo #22663) or the Pierce BCA Protein Assay Kit (Thermo #23225) in a 96-well plate, according to manufacturer's protocol. Samples were diluted to the same final concentration, mixed with 1x Orange G dye (Sigma #O3756) containing 10% β-mercaptoethanol (Sigma #M3148) and incubated 10 min at 100 ºC before loading. Precast 4-15% TGX protein gels (Bio-Rad #4561086) were loaded with 10-20 µg of total protein lysate and run for 1h at 135V. Proteins were transferred to 0.45 µm nitrocellulose membrane (Bio-Rad #1704271) with a Trans-Blot Turbo Transfer system (Bio-Rad) using the pre-determined high molecular weight transfer protocol (10 min, 2.5 A constant). Blocking of the membrane was performed using Intercept (TBS) Blocking Buffer (LI-COR #927-60001) for at least 1h at room temperature. Incubation with primary antibodies (all diluted 1:1000 in blocking buffer containing 0.1% Tween-20) was carried out overnight at 4 ºC. Rabbit anti-SYNGAP1 (Cell Signaling Technology #5539S), rabbit anti-STXBP1 (Munc18-1, Cell Signaling Technology #13414S), mouse anti-phospho-ERK1/2 (Cell Signaling Technology #9106), rabbit anti-ERK1/2 (Cell Signaling Technology #9102) and mouse anti-ATP5F1 (Abcam #ab117991) were used. Membrane was then rinsed with 1x Tris-buffered saline with 0.1% Tween (TBST) 4 times for 5 min. Incubation with secondary antibodies (diluted 1:10,000 in blocking buffer containing 0.1% Tween-20) was performed at room temperature for 1h. For STXBP1 and ERK blots, IRDye 680RD anti-rabbit (LI-COR #926-68073) and IRDye 800CW anti-mouse (LI-COR #926-32212) were used. For SYNGAP1 blots, IRDye 800CW anti-rabbit (LI-COR #926-32213) and IRDye 680RD anti-mouse (LI-COR #926-68072)

were used. Membrane was rinsed again with 1x TBST 4 times for 5 min and imaged on Odyssey Imager (LI-COR) using a resolution of 169 µm.

Western blot quantifications were normalized to ATP5F1 according to LI-COR's Housekeeping Protein Normalization Protocol. A standard curve was included in each blot to ensure assay linearity.

Behavioral assessments

Animals were transported in their home cages to testing room(s), habituated for 1-2 hours, and all testing apparatuses were thoroughly disinfected before testing and between animals. At 4-weeks and 30-weeks of age, animals were weighed and underwent open field, elevated plus maze, and horizontal ladder testing on nonconsecutive days. For open field testing, animals were individually placed in well-lit, 10.75 x 10.75 x 8 inch plexiglass chambers which were housed in a sound attenuating cubicles (Med Associates Inc., ENV-51050-A). Animals were tracked for 30 minutes using Activity Monitor (Med Associates Inc, Version 6.02) to assess; overall activity levels via total distance traveled, stereotypy (abnormal repetitive behaviors) via number of stereotypic events, and anxiety-like behaviors via time spent in the center of the testing chamber. As an additional test for anxiety-like and exploratory behaviors, elevated plus maze was performed. Animals were individually placed in the center of the maze, continuously recorded for 10 minutes, and tracked using ANY-Maze (version 6.0). Center of mass was used to quantify the time in open arms and number of open arm entries.

Horizontal ladder testing was used to assess locomotor coordination and precision. A 64 cm long ladder with rungs spaced 2 cm apart was elevated 17 cm above the testing table and a hollow black escape box placed at one end. Animals were placed at the starting (open) end of the ladder and following a successful pass were kept in the dark escape box for 1-2 minutes before starting the next pass. Following a "training" pass to familiarize animals with the apparatus and escape box, 5 successful passes were recorded. Passes were considered successful if the animal traversed the ladder without turning around or pausing for >2 seconds. If unsuccessful, animals were replaced at the start. The same blinded observer scored all videos and foot slips were counted if the animal's paw broke the plane of the ladder rungs.

To assess spatial learning and memory, animals underwent Barnes maze testing consisting of 4 training days and 1 test day, at 5-weeks and 31-weeks of age. The Barnes Maze table (San Diego Instruments; 36 inch diameter table; 20, 2 inch holes) was positioned in the center of well-lit room with black walls, discrete visual cues (large white shapes) on each of the 4 walls, and a video camera positioned directly above the table. Videos were recorded and analyzed using ANY-Maze (version 7.3). On training days all holes were occluded except the "target hole" which was unblocked, allowing mice to enter a dark escape box. The target hole remained in the same position for each animal during training days and was changed every 4 animals to minimize the influence of any unknown cues or preferences. Training days consisted of two non-consecutive trials during which animals were placed in the middle of the table and covered with a cardboard box (15 cm x 15 cm) for 1 minute to habituate. The box was removed and the animal recorded for 150 seconds. If the animal did not successfully enter the target hole after 150 seconds, it was gently guided into the target hole and remained there for 60 seconds. On the test day, the target hole was occluded, and animals were recorded for a single 150 second trial.

Primary cortical neuron isolations and ASO treatments

Primary cortical neurons were isolated at embryonic day 16-18 from pregnant *Syngap1*$^{Hu/Hu}$ females crossed with *Syngap1*$^{+/-}$ males. Cortical tissue was isolated from individual embryos in 1x HBSS (Gibco #14170-112) supplemented with 1% Penicillin/Streptomycin (Gibco #15140122), 1% HEPES (Gibco #15630080) and 1% Sodium Pyruvate (Gibco #11360070) and cut into small pieces (~2 mm). Cortices were stored on ice and pooled based on genotyping. In brief, DNA from embryos was extracted using the Kapa Mouse genotyping kit (Roche #41106300) and diluted 1:100 for qPCR using SYBR Green (Bio-RAD #1725271) with recommended primers from Jax (strain #008890) to detect the presence of the WT or null *Syngap1* allele. Cortices were digested via incubation in 20 U/mL Papain plus DNase (Worthington Biochemical Corporation, #LK003178 and #LK003172) for 15-20 minutes at 37°C in 1X HBSS with supplements. Digestion was halted by the addition of 10% Heat inactivated-FBS (Corning #MT35-010-

CV) and washed once in Neurobasal media (Gibco #21103049) and then Neurobasal supplemented with 1% B27 Plus (Gibco #A3582801), 1% GlutaMax (Gibco #35050061), and 1% Penicillin/Streptomycin. Cortices were manually dissociated into single cells by trituration with a 5 ml Serological pipette 3-4 times followed by 25-30 times with a p1000 pipette tip in 2-3 mL of supplemented Neurobasal media. Live cells were counted with trypan blue on a hematocytometer. Cells (200,000) were seeded in 24-well plates (Corning #353226). Plates were coated with 50 µg/mL of poly-D-lysine (Sigma-Aldrich #P1149) in 0.1 M Borate Buffer, pH 8.5 in a sterile environment over night at room temperature. The next day, plates were washed at least 3 times in sterile H_2O and incubated in a humidified environment at 37°C in 5% CO2 in supplemented Neurobasal media with 5 µg/mL of laminin (Gibco #23017015). After seeding, cells were incubated in a humidified environment at 37°C in 5% CO_2, and the following day media was changed. Subsequently, 50% media changes were performed once per week until day in vitro (DIV) 10, and twice a week thereafter.

ASO treatments were performed via gymnotic delivery of the ASO in DIV5-7 *Syngap1*$^{Hu/-}$ primary neurons for 7 days. ASOs were purchased from IDT and sequences can be found in **Supplementary Data 1**.

Statistical analyses

Measurements were taken from distinct samples. The number of samples is stated explicitly in the figure and represented as individual data points for bar graphs. Kaplan–Meier survival curves were used to represent the survivability of the different model mice and the Mantel–Cox (Log-rank) test was used to statistically compare the overall survival between groups. Statistical significance was defined as $p < 0.05$. Data plots and statistical analyses were performed in GraphPad Prism 10.1 software. Individual statistical tests applied to each data set are given in the respective figure legends. Data are represented as mean values ± standard error of the mean (SEM) and behavioral data are represented as mean values ± 1 standard deviation (SD).

Results

Generation of a knock-in *Syngap1* humanized mouse model

The *Syngap1* humanized mouse is a non-conditional KI model in which the mouse *Syngap1* locus was replaced with the human *SYNGAP1* gene (**Figure 1A**). We generated hybrid (*Syngap1*$^{Hu/+}$), fully humanized (*Syngap1*$^{Hu/Hu}$) and wild-type littermate (*Syngap1*$^{+/+}$) animals for which we confirmed the presence of 1, 2 and 0 copies of the human *SYNGAP1* transgene in the targeted mouse locus, respectively, using a CNV qPCR assay (**Figure 1B**). Grossly, hybrid and humanized *Syngap1* mice were indistinguishable from pure wild-type littermates.

We conducted a 36-week-long survivability study including male and female mice with hybrid, fully humanized and wild-type genotypes. Mouse viability was not affected in hybrid nor fully humanized *Syngap1* mice, indicating that both mono- and bi-allelic humanization of the *Syngap1* locus are well tolerated. Body weights and growth rates were similar between all *Syngap1* genotypes (**Figure 1C**). We also evaluated potential deviations of genotype distributions from the expected normal Mendelian inheritance among weaned pups. Genotypic ratios were calculated from the offspring of *Syngap1* hybrid matings (*Syngap1*$^{Hu/+}$ x *Syngap1*$^{Hu/+}$), which should result in 50% of *Syngap1*$^{Hu/+}$, 25% of *Syngap1*$^{Hu/Hu}$ and 25% of *Syngap1*$^{+/+}$ mice. The observed genotypic ratios for *Syngap1* mice followed normal Mendelian inheritance (**Figure 1D**).

We characterized the *Syngap1* humanized mouse model at the RNA and protein level with samples isolated from cerebral cortex. *Syngap1*$^{Hu/Hu}$ mice expressed only human *SYNGAP1* transcript, while *Syngap1*$^{Hu/+}$ showed a ~50% reduction in human *SYNGAP1* mRNA levels relative to *Syngap1*$^{Hu/Hu}$, as expected (**Figure 1E**, middle panel). Human *SYNGAP1* expression was also inversely correlated with mouse *Syngap1* expression, confirming successful humanization of the locus (**Figure 1E**, left panel). Using a cross-reactive qPCR assay to detect both mouse and human *SYNGAP1* transcripts, we observed a 1.4x increase in total *SYNGAP1* mRNA in both *Syngap1*$^{Hu/+}$ and *Syngap1*$^{Hu/Hu}$ mice (**Figure 1E**, right panel). These data indicate that *SYNGAP1* is efficiently transcribed following humanization of its genomic locus. We performed western blotting using a SYNGAP1 antibody raised against a fully conserved region of the protein surrounding Arg1070 (mouse and human SYNGAP1 are 99% conserved at the amino acid level). *Syngap1*$^{Hu/Hu}$ showed a ~35% increase in total SYNGAP1 protein levels relative to wild-type littermates, with a subtler potential increase in expression with mono-allelic humanization (**Figure 1F**). These data point towards modestly enhanced transcription of the human *SYNGAP1* gene and/or increased stability of the human *SYNGAP1* mRNA as a plausible explanation for SYNGAP1 protein upregulation in fully humanized mice.

Generation of a knock-in *Stxbp1* humanized mouse model

Similarly, the *Stxbp1* humanized mouse model was generated by replacing the mouse *Stxbp1* locus with the human *STXBP1* gene (**Figure 2A**). We confirmed the presence of the expected copies of human *STXBP1* transgene in *Stxbp1*$^{Hu/+}$ (1 copy), *Stxbp1*$^{Hu/Hu}$ (2 copies) and *Stxbp1*$^{+/+}$ mice (0 copies) (**Figure 2B**). In terms of physical appearance, *Stxbp1* model mice occasionally presented abnormal tail morphologies (i.e. kinked tails).

Bi-allelic humanization of the *Stxbp1* gene significantly reduced viability. Male *Stxbp1*$^{Hu/Hu}$ presented an abrupt ~90% mortality rate around 9 weeks of age, while *Stxbp1*$^{Hu/Hu}$ females showed a milder, more stepwise mortality phenotype with a ~30% mortality at 36 weeks (**Figure 2C**). However, these observations were not recapitulated in either male or female *Stxbp1*$^{Hu/+}$ mice that carry only one copy of the human *STXBP1* gene, suggesting that mono-allelic but not bi-allelic humanization is well tolerated (**Figure 2C**). Male *Stxbp1*$^{Hu/Hu}$ mice body weights were not significantly different from hybrid or wild-type littermates and confirmed the absence of weight loss preceding mortality, discarding growth impairments as a potential cause of death (**Figure 2D**). When evaluating the genotypic distribution from the offspring of *Stxbp1* hybrid matings (*Stxbp1*$^{Hu/+}$ x *Stxbp1*$^{Hu/+}$), we observed a significant underrepresentation in the number of weaned *Stxbp1*$^{Hu/Hu}$ mice (~15% of the offspring) relative to the expected 25% Mendelian ratio (**Figure 2E**). These data suggest ~40% embryonic lethality in *Stxbp1*$^{Hu/Hu}$ mice.

In molecular characterizations from cerebral cortex tissue, *Stxbp1*$^{Hu/Hu}$ mice presented only human *STXBP1* mRNA, concomitant with a lack of expression of the mouse gene, confirming successful humanization (**Figure 2F**, left and middle panels). Cross-reactive qPCR did not detect significant differences in total *STXBP1* mRNA levels across the different genotypes (**Figure 2F**, right panel). When assessing STXBP1 protein abundance (100% conservation of STXBP1 amino acid sequence between mouse and human), we observed a ~40% reduction in STXBP1 protein levels in *Stxbp1*$^{Hu/Hu}$ mice relative to wild-type littermates (**Figure 2G**). Surprisingly, the reduction in STXBP1 levels was not human gene dosage-sensitive, since STXBP1 protein abundance was not altered in *Stxbp1*$^{Hu/+}$ mice (**Figure 2G**). The STXBP1 downregulation observed in *Stxbp1*$^{Hu/Hu}$ cannot be explained by a transcriptional regulatory mechanism, since total *STXBP1* mRNA levels were unaffected in these mice. Post-transcriptional dysregulation of the human *STXBP1* mRNA in the murine context may contribute to reduced expression, as could the insertion of additional human genomic elements not naturally present in the mouse genome such as miR-3911 and a lncRNA encoded in the reverse strand (see **Figure 2A**). Yet, such dysregulation would be expected to produce an intermediate reduction in protein expression in *Stxbp1*$^{Hu/+}$ mice, which was not observed. This raises the possibility that reduced *STXBP1* expression may be a secondary consequence of an unanticipated, pathogenic phenotype resulting from bi-allelic humanization of this locus.

Given that the original *Stxbp1*$^{Hu/Hu}$ animals in a pure C57BL/6J genetic background were not viable until they underwent a one-generation outcross with the BALB/c strain, we investigated whether further outcrossing to BALB/c could improve *Stxbp1*$^{Hu/Hu}$ viability. After outcrossing to BALB/c for two additional generations, *Stxbp1*$^{Hu/+}$ mice with a 3x outcrossed background were subsequently bred together to obtain fully humanized animals. The observed Mendelian ratio for the 3x outcrossed *Stxbp1*$^{Hu/Hu}$ was ~3% (**Figure S1**), ~5-fold lower than that in the 1x (original) model (~15%) (**Figure 2E**) and thus representing an unexpected increase in embryonic lethality. Finally, we attempted the generation of a *Stxbp1* humanized-disease mouse model by crossing our *Stxbp1*$^{Hu/+}$ or *Stxbp1*$^{Hu/Hu}$ mice (in 1x and 3x backgrounds) with *Stxbp1* heterozygous knockout mice (*Stxbp1*$^{+/-}$, B6;129S-Stxbp1tm1Sud/J) (8). Unfortunately, these matings did not produce offspring with *Stxbp1*$^{Hu/-}$ genotypes, precluding the generation of an *Stxbp1* humanized haploinsufficiency model.

Syngap1 **humanized-haploinsufficient mice**

To generate a Syngap1-disease mouse model which would recapitulate disease-linked behavioral phenotypes and allow for testing of human gene-targeted therapies, we crossed the *Syngap1*$^{Hu/Hu}$ mice generated here with *Syngap1*-heterozygous (and haploinsufficient) mice generated by Kim et al (*Syngap1*$^{+/-}$, B6;129-Syngap1^{tm1Rlh}/J) in which exons 7 and 8 of *Syngap1* are deleted, resulting in the introduction of a premature termination codon (12) (**Figure 3A**). These matings produced equal ratios (~50% each) of *Syngap1* humanized-haploinsufficient mice (*Syngap1*$^{Hu/-}$) and hybrid control littermates (*Syngap1*$^{Hu/+}$) (**Figure 3A**), indicating no embryonic lethality. Both genotypes were physically identical and weekly body weights up to 15 weeks of age showed that *Syngap1*$^{Hu/-}$ and *Syngap1*$^{Hu/+}$ animals were similar in growth rate and size (**Figure 3B**).

Cross-reactive RT-qPCR of hemi-brain RNA extracts from *Syngap1*$^{Hu/-}$ revealed a ~30% reduction in total (mouse and human) *SYNGAP1* mRNA relative to hybrid controls (*Syngap1*$^{Hu/+}$) (**Figure 3C, left**), suggesting that mutant *Syngap1* mRNA is being degraded by nonsense-mediated decay (NMD) due to the presence of a premature termination codon [for review on NMD, see ref. (21)]. As a control, we also observed a reduction in *Syngap1* mRNA levels (~20%) in *Syngap1*$^{+/-}$ mice relative to wild-types (**Figure 3C, right**), which is in agreement with previous qPCR-based RNA characterizations of this mouse model (22). However, it is worth noting that recent brain RNA-seq studies did not detect significant differences in total *Syngap1* mRNA levels between *Syngap1*$^{+/-}$ and *Syngap1*$^{+/+}$ mice when considering the abundance of all the possible splice junctions (i.e. naturally occurring N- and C-terminal *Syngap1* isoforms), suggesting that some isoforms may escape from NMD or that they may be upregulated in a compensatory manner (22).

At the protein level, Western blotting showed a ~50% reduction in total SYNGAP1 protein levels in *Syngap1*$^{Hu/-}$ hemi-brain tissue, similar to the decrease seen in *Syngap1*$^{+/-}$ *mice* compared to WT controls

(**Figure 3D**). The absence of full SYNGAP1 protein and/or truncated protein species produced by the null allele indicated that the mutant transcripts are either translationally inactive or generate a truncated protein that is readily degraded. In addition, given SYNGAP1's role as a negative regulator of the Ras-Raf-MEK-ERK signaling pathway (13, 23), we examined ERK signaling in *Syngap1* model mice by looking at basal levels of phosphorylated, or active, ERK (p-ERK) relative to total ERK abundance. *Syngap1*$^{Hu/-}$ mice displayed an apparent ~20% increase in p-ERK over total ERK relative to *Syngap1*$^{Hu/+}$ (**Figure 3E**), consistent with our observations in *Syngap1*$^{+/-}$ vs. *Syngap1*$^{+/+}$ (**Figure 3E**). While these data are not statistically significant, previous studies reported a more consistent p-ERK elevation in a *Syngap1* heterozygous knockout mouse model (22). The specific genetic background of the animals used for the characterization or minor differences in experimental protocols may account for the increased variability observed in our hands. These data demonstrate the successful generation of a *Syngap1* mouse model that expresses haploinsufficient levels of human SYNGAP1.

Syngap1 humanized-haploinsufficient mice exhibit age-dependent behavioral phenotypes

To characterize behavioral phenotypes at multiple ages, juvenile (4 to 5 weeks old) and adult (30 to 31 weeks old) male and female *Syngap1*$^{Hu/+}$ and *Syngap1*$^{Hu/-}$ underwent a series of locomotor and cognitive tests. 30-minute open field assays showed an increase in total distance traveled (**Figure 4A,** left) and in stereotypic behaviors (**Figure 4B,** left) (24) in juvenile *Syngap1*$^{Hu/-}$ mice, indicating hyperactivity and cognitive dysfunction in line with previous behavioral characterizations of non-humanized *Syngap1* haploinsufficient mouse models (22, 25). However, these phenotypes were not recapitulated in adult *Syngap1*$^{Hu/-}$ mice (**Figure 4A&B,** right). Neither juvenile nor adult mice exhibited differences in anxiety-like behaviors in the open field test, as determined by time spent in the center of the arena (**Figure 4C**). As other mouse models of Syngap1 haploinsufficiency display reduction in anxiety-like behaviors (25–27), elevated plus maze test was also used to further probe these behaviors. We did not observe any differences between *Syngap1*$^{Hu/+}$ and *Syngap1*$^{Hu/-}$, irrespective of age, in either the number of open arm entries or time spent in open arms of the maze (**Figure 4D&E**), confirming a lack of an anxiety phenotype in the humanized-haploinsufficient mice. Next, we evaluated locomotor coordination and precision using a horizontal ladder test. While no differences were seen in juvenile mice, adult *Syngap1*$^{Hu/-}$ had significantly more foot slips compared to *Syngap1*$^{Hu/+}$ mice (**Figure 4F**). Similarly, Muhia et al (28) and Nakajima et al (27) found deficits in locomotor adaptation in 12- and 53-week-old mice via accelerating rotarod. Therefore, locomotor phenotypes likely represent an age-dependent phenotype and may arise from aberrant plasticity during a period of heightened locomotor plasticity from P30-60 (29). Finally, we performed the Barnes maze test to assess rodent spatial learning and memory. During the learning phase of the Barnes Maze (first four days), no differences were seen between *Syngap1*$^{Hu/+}$ and *Syngap1*$^{Hu/-}$ at either age when time to enter the target hole was measured (**Figure 4G**). However, on the fifth day (test day), *Syngap1*$^{Hu/-}$ mice took significantly longer to contact the target hole, indicating impaired spatial memory and/or diminished memory recall (**Figure 4H**). These findings show that *Syngap1* humanized-haploinsufficient mice recapitulate several behavioral phenotypes associated with SYNGAP1 disorder, some of which are age dependent.

Human *SYNGAP1*-targeted ASOs modulate *SYNGAP1* expression in the context of *Syngap1*$^{Hu/-}$

Our final goal was to determine whether human *SYNGAP1* expression could be modulated in the *Syngap1* humanized-haploinsufficient mouse model using a human-specific *SYNGAP1* therapy. We and others had previously identified an alternative 3' splice site (Alt. 3'ss) event in *SYNGAP1* exon 10-11 that promotes NMD and restricts *SYNGAP1* expression across numerous cell types, including iPSC-neurons (**Figure 5A**) (16, 17). This Alt. 3'ss event is dependent on the binding of polypyrimidine tract binding proteins (PTBPs) to *SYNGAP1* pre-mRNA, opening the opportunity for a therapeutic splice switching strategy using steric-blocking ASOs to specifically disrupt PTBP binding and upregulate *SYNGAP1* (**Figure 5A**). Our previous study identified two main ASO candidates named ET-019 and ET-085 targeting PTBP binding sites located upstream (Site-1) and downstream (Site-2) from the Alt. 3'ss, respectively, that redirected splicing and increased *SYNGAP1* mRNA abundance in SYNGAP1 patient-derived iPSC-neurons (17). Here we tested these human-specific compounds in *Syngap1*$^{Hu/-}$ -derived primary neurons to examine their ability to upregulate human *SYNGAP1*. Gymnotic delivery of ET-019 and ET-085 in *Syngap1*$^{Hu/-}$ -derived primary neurons was well tolerated and significantly increased *SYNGAP1* mRNA abundance (1.7- and 1.5-fold, respectively) relative to mock-treated cells or a negative control ASO (ET-

SC2) with the same length and chemistry (**Figure 5B**). This indicated effective human target engagement and demonstrated that ASO-mediated PTBP disruption in both Site-1 and Site-2 can improve human *SYNGAP1* expression in this mouse model. In follow-up ASO testing, we found that ET-019 upregulated human *SYNGAP1* in a dose-dependent fashion, reaching a ~2.9-fold increase at 20 µM concentration (**Figure 5C**). In parallel, we also investigated whether *SYNGAP1* expression could be downregulated using a gapmer ASO (Gap-SYN) specifically designed to trigger RNase H1-mediated degradation of human *SYNGAP1* mRNA. *Syngap1*$^{Hu/-}$ primary neurons treated with Gap-SYN showed a strong reduction (~70%) in *SYNGAP1* mRNA levels, confirming successful knockdown of the target (**Figure 5B**). Together, our data indicates that *SYNGAP1* expression can be modulated bidirectionally in the humanized haploinsufficiency context using human gene-targeted ASOs.

Discussion

Here we generated *Syngap1* and *Stxbp1* humanized mouse models to provide novel platforms for therapeutic development in SYNGAP1 and STXBP1 disorders. For both mouse models, the humanization also includes upstream (promoter and proximal enhancers) and downstream (3'UTR) regulatory regions, enabling testing of human-specific therapies targeting these elements. We also generated a *Syngap1* humanized-disease mouse model that is haploinsufficient and recapitulates several SYNGAP1-related phenotypes. Finally, we show that human gene-targeted ASOs can effectively modulate human *SYNGAP1* expression in this *Syngap1* humanized-haploinsufficient mouse model.

The *Syngap1* humanized mouse colony can be maintained as *Syngap1*$^{Hu/Hu}$ and be rapidly expanded due to its Mendelian inheritance and normal viability and lifespan. It is worth noting that *Syngap1* humanization also includes the human *SYNGAP1* antisense transcript (*SYNGAP1-AS*), which may modulate *SYNGAP1* expression and thus be a potential therapeutic target that is only available in these humanized animals. The *Syngap1*$^{Hu/Hu}$ mouse model is well suited for the generation of humanized-disease models, which was generated here by crossing the humanized model with available *Syngap1*$^{+/-}$ mouse models. Alternatively, this may be accomplished by introducing heterozygous, human pathogenic variants directly into the *Syngap1*$^{Hu/Hu}$ background via CRISPR/Cas genome editing.

The initial *Stxbp1*$^{Hu/Hu}$ animals on a pure C57BL/6J background were non-viable until outcrossed with BALB/c, generating the mouse model characterized here. While the genetic cause for the impaired viability of *Stxbp1*$^{Hu/Hu}$ mice (especially males) is unclear, we hypothesized that further increasing genetic variability would improve viability. However, further outcrossing to BALB/c did not ameliorate (and perhaps worsened), embryonic lethality, indicating that the frailty of this mouse model is not related to genetic background diversity. Due to the impaired viability and reduced *STXBP1* expression in *Stxbp1*$^{Hu/Hu}$ mice, a *Stxbp1* humanized-haploinsufficient mouse model (*Stxbp1*$^{Hu/-}$) could not be generated, as evidenced by the absence of *Hu/-* genotypes in the offspring of *Stxbp1*$^{Hu/Hu}$/*Stxbp1*$^{Hu/+}$ x *Stxbp1*$^{+/-}$ matings. This lack of a *Stxbp1* humanized-haploinsufficient model precludes evaluation of phenotypic rescue after therapeutic intervention with human gene-targeted approaches. However, *Stxbp1*$^{Hu/+}$ mice are viable and express normal levels of STXBP1, providing a useful model to assess human target engagement and mechanistic interrogations of clinical drug candidates. Using *Stxbp1*$^{Hu/+}$ mice, we have successfully detected human *STXBP1* engagement and upregulation after treatment with a variety of therapeutic approaches targeting the 5' or 3' regulatory regions of the human gene (data not shown), illustrating the utility of the *Stxbp1* humanized model for certain pre-clinical studies.

For pre-clinical development of human *SYNGAP1*-targeted therapeutics, we generated a *Syngap1* humanized-disease mouse model that is viable, displays normal growth rates, and is haploinsufficient (**Figure 3A, B & D**). This suggests that human SYNGAP1 protein (~99% homologous to mouse SYNGAP1) is fully functional in the mouse context. All *Syngap1*$^{Hu/-}$ animals generated here showed consistent SYNGAP1 loss-of-function, but we note a weak inverse correlation between SYNGAP1 and active ERK levels in this mouse model as indicated by phosphorylation of ERK. As phospho-ERK detection is variable, it may not be a sensitive measure to determine downstream molecular rescue upon therapeutic upregulation of human SYNGAP1 (**Figure 3E**). Alternative cellular phenotypes such as AMPA receptor trafficking or dendritic spine morphology (30) may represent more sensitive measures to detect downstream rescue of human SYNGAP1 haploinsufficiency.

Consistent with the original *Syngap1*$^{+/-}$ mice generated by Kim et al. (12), the *Syngap1*$^{Hu/-}$ generated here recapitulate disease-linked phenotypes, including hyperactivity, increased repetitive behaviors, and memory deficits (**Figure 4 A, B & H**) (25, 31, 32). However, adult *Syngap1*$^{Hu/-}$ mice were not hyperactive at 30 weeks of age, which is inconsistent with other aged *Syngap1*-disease mouse models (11, 27). Deficits in locomotor coordination and precision emerged in adult *Syngap1*$^{Hu/-}$, coinciding with deficits in locomotor adaptation in adult *Syngap1*$^{+/-}$ mice (14, 27). Thus, age-related locomotor deficits may result from either poor motor commands or the inability for sensory feedback to make appropriate adjustments while locomotion is ongoing in these tasks.

Surprisingly, neither juvenile nor adult *Syngap1*$^{Hu/-}$ showed decreased anxiety-like behaviors (increased exploratory behaviors) (**Figure 4C & D**), which are consistently seen across mouse *Syngap1*-disease models (14, 27, 31, 32). The lack of anxiety-related phenotypes and other age-dependent phenotypes

may result from differences in human *SYNGAP1* transcripts having increased stability or improved intracellular trafficking relative to mouse transcripts, allowing for a small increase in protein production beyond that of endogenous mouse alleles, as seen in *Syngap1*$^{Hu/Hu}$ mice (**Figure 1F**). This small increase may be enough to alter the neurocircuitry and neurophysiology underlying disease phenotypes. Importantly, this could indicate that a modest upregulation in SYNGAP1 protein may provide some therapeutic benefit. Lastly, mouse genetic background is known to impact behavioral phenotypes in neurodevelopmental disease models (3, 33). As *Syngap1*$^{Hu/-}$ and *Syngap1*$^{Hu/+}$ mice for behavioral testing were on a C57BL/6J background, it is plausible that outcrossing to other strains may impact disease-related behavioral phenotypes.

Finally, we demonstrate that human *SYNGAP1* expression can be bidirectionally modulated in the humanized-haploinsufficient mouse context. In *Syngap1*$^{Hu/-}$ primary neurons, a gapmer ASO effectively engages with human *SYNGAP1* and triggers its degradation. Importantly, we also show that two previously identified human-specific ASOs (ET-019 and ET-085) (17) increase human *SYNGAP1* mRNA abundance, one of which does so in a dose-dependent manner (**Figure 5C**). As these splice-switching ASOs act through PTBP disruption (17), these data suggest that mouse PTBP proteins can also recognize and regulate the alternative 3' splicing event of human *SYNGAP1* (16). Ultimately, the *Syngap1*$^{Hu/-}$ mouse model generated here will enable future *in vivo* studies to evaluate efficacy and phenotypic rescue with various human gene-targeted strategies, thereby accelerating the arrival of these therapies to patients.

References

1. J. A. López-Rivera, *et al.*, A catalogue of new incidence estimates of monogenic neurodevelopmental disorders caused by de novo variants. *Brain* **143**, 1099–1105 (2020).

2. M. Weldon, M. Kilinc, J. Lloyd Holder, G. Rumbaugh, The first international conference on SYNGAP1-related brain disorders: A stakeholder meeting of families, researchers, clinicians, and regulators. *J Neurodev Disord* **10**, 1–6 (2018).

3. J. Kovačević, *et al.*, Protein instability, haploinsufficiency, and cortical hyper-excitability underlie STXBP1 encephalopathy. *Brain* **141**, 1350–1374 (2018).

4. M. H. Berryer, *et al.*, Mutations in SYNGAP1 Cause Intellectual Disability, Autism, and a Specific Form of Epilepsy by Inducing Haploinsufficiency. *Hum Mutat* **34**, 385–394 (2013).

5. D. R. M. Vlaskamp, *et al.*, SYNGAP1 encephalopathy: A distinctive generalized developmental and epileptic encephalopathy. *Neurology* **92**, E96–E107 (2019).

6. J. Xian, *et al.*, Assessing the landscape of STXBP1-related disorders in 534 individuals. *Brain* **145**, 1668–1683 (2022).

7. H. Stamberger, *et al.*, STXBP1 encephalopathy: A neurodevelopmental disorder including epilepsy. *Neurology* **86**, 954–962 (2016).

8. M. Verhage, *et al.*, Synaptic assembly of the brain in the absence of neurotransmitter secretion. *Science* **287**, 864–869 (2000).

9. W. Chen, *et al.*, Stxbp1/Munc18-1 haploinsufficiency impairs inhibition and mediates key neurological features of STXBP1 encephalopathy. *Elife* **9** (2020).

10. H. Miyamoto, *et al.*, Potentiation of excitatory synaptic transmission ameliorates aggression in mice with Stxbp1 haploinsufficiency. *Hum Mol Genet* **26**, 4961–4974 (2017).

11. Y. Araki, *et al.*, Mouse models of SYNGAP1-related intellectual disability. *Proc Natl Acad Sci U S A* **120**, e2308891120 (2023).

12. J. H. Kim, H. K. Lee, K. Takamiya, R. L. Huganir, The role of synaptic GTPase-activating protein in neuronal development and synaptic plasticity. *J Neurosci* **23**, 1119–1124 (2003).

13. N. H. Komiyama, *et al.*, SynGAP Regulates ERK/MAPK Signaling, Synaptic Plasticity, and Learning in the Complex with Postsynaptic Density 95 and NMDA Receptor. *The Journal of Neuroscience* **22**, 9721–9732 (2002).

14. M. Muhia, *et al.*, Molecular and behavioral changes associated with adult hippocampus-specific SynGAP1 knockout. *Learn Mem* **19**, 268–281 (2012).

15. P. D. Galer, *et al.*, Quantitative EEG Spectral Features Differentiate Genetic Epilepsies and Predict Neurologic Outcomes. *medRxiv* (2024). https://doi.org/10.1101/2024.10.09.24315105.

16. R. Yang, *et al.*, Upregulation of SYNGAP1 expression in mice and human neurons by redirecting alternative splicing. *Neuron* **111**, 1637-1650.e5 (2023).

17. J. M. Dawicki-McKenna, *et al.*, Mapping PTBP2 binding in human brain identifies SYNGAP1 as a target for therapeutic splice switching. *Nature Communications 2023 14:1* **14**, 1–20 (2023).

18. K. H. Lim, *et al.*, Antisense oligonucleotide modulation of non-productive alternative splicing upregulates gene expression. *Nature Communications 2020 11:1* **11**, 1–13 (2020).

19. Y. Cao, *et al.*, RNA-based translation activators for targeted gene upregulation. *Nat Commun* **14** (2023).

20. B. Torkzaban, R. Kawalerski, J. Coller, Development of a Tethered mRNA Amplifier to increase protein expression. *Biotechnol J* **17** (2022).

21. S. Lykke-Andersen, T. H. Jensen, Nonsense-mediated mRNA decay: An intricate machinery that shapes transcriptomes. *Nat Rev Mol Cell Biol* [Preprint] (2015).

22. Y. Araki, *et al.*, Mouse models of SYNGAP1-related intellectual disability. *Proc Natl Acad Sci U S A* **120** (2023).

23. G. Rumbaugh, J. P. Adams, J. H. Kim, R. L. Huganir, SynGAP regulates synaptic strength and mitogen-activated protein kinases in cultured neurons. *Proc Natl Acad Sci U S A* (2006).

24. J. Novak, J. D. Bailoo, L. Melotti, H. Würbel, Effect of Cage-Induced Stereotypies on Measures of Affective State and Recurrent Perseveration in CD-1 and C57BL/6 Mice. *PLoS One* **11** (2016).

25. X. Guo, *et al.*, Reduced expression of the NMDA receptor-interacting protein SynGAP causes behavioral abnormalities that model symptoms of Schizophrenia. *Neuropsychopharmacology* **34**, 1659–1672 (2009).

26. M. Kilinc, *et al.*, Species-conserved SYNGAP1 phenotypes associated with neurodevelopmental disorders. *Mol Cell Neurosci* **91**, 140–150 (2018).

27. R. Nakajima, *et al.*, Comprehensive behavioral analysis of heterozygous Syngap1 knockout mice. *Neuropsychopharmacol Rep* **39**, 223–237 (2019).

28. M. Muhia, B. K. Yee, J. Feldon, F. Markopoulos, I. Knuesel, Disruption of hippocampus-regulated behavioural and cognitive processes by heterozygous constitutive deletion of SynGAP. *Eur J Neurosci* **31**, 529–543 (2010).

29. T. Kim, B. M. Hooks, Developmental timecourse of aptitude for motor skill learning in mouse. *bioRxiv* (2024). https://doi.org/10.1101/2024.07.19.604309.

30. Y. Araki, M. Zeng, M. Zhang, R. L. Huganir, Rapid Dispersion of SynGAP from Synaptic Spines Triggers AMPA Receptor Insertion and Spine Enlargement during LTP. *Neuron* **85**, 173–189 (2015).

31. T. A. Fenton, *et al.*, Hyperexcitability and translational phenotypes in a preclinical mouse model of SYNGAP1-related intellectual disability. *Transl Psychiatry* **14**, 405 (2024).

32. V. Verma, *et al.*, Pharmacological intervention in young adolescents rescues synaptic physiology and behavioural deficits in Syngap1+/- mice. *Exp Brain Res* **240**, 289–309 (2022).

33. M. Rubinstein, *et al.*, Genetic background modulates impaired excitability of inhibitory neurons in a mouse model of Dravet syndrome. *Neurobiol Dis* **73**, 106–117 (2015).

Figure legends

Figure 1. Generation of the *Syngap1* humanized mouse model. (**A**) Cartoon depicting the *Syngap1* locus after humanization. FRT and F3 are two heterotypic recognition sequences used for FLP-mediated neomycin and hygromycin cassette removal. The human *SYNGAP1* transgene is flanked with loxP sites. 5' regulatory region indicates promoter and proximal enhancers. (**B**) qPCR from gDNA of wild-type (+/+), hybrid (Hu/+) and fully humanized (Hu/Hu) *Syngap1* mice. *Tert* was used as endogenous control. (**C**) Body weights of *Syngap1* model mice. (**D**) Genotypic ratios from the offspring of *Syngap1*$^{Hu/+}$ x *Syngap1*$^{Hu/+}$ breedings. Cartoon was created with BioRender. (**E**) RT-qPCR from cerebral cortex tissue of 9-week-old *Syngap1* model mice. *Atp5f1* mRNA was used as endogenous control. (**F**) SYNGAP1 western blot from samples in (**E**). ATP5F1 was used as endogenous control. (**B**, **C**, **E** and **F**) Data are represented as mean values ± SEM. Data points represent independent biological replicates. (**E** and **F**) White and gray data points indicate females and males, respectively. (**B, E** and **F**) One-way ANOVA with Dunnett's multiple comparison test vs. wild-type (+/+). (**C**) 2-way ANOVA with Dunnett's multiple comparison test vs. wild-type (+/+) (**D**) Chi-square test (df = 2, n = 45, p = 0.9048). *SYNGAP1-AS*, *SYNGAP1* antisense transcript. FC, fold change. ns, non-statistically significant.

Figure 2. Generation of the *Stxbp1* humanized mouse model. (A) Cartoon depicting the *Stxbp1* locus after humanization. FRT and F3 are two heterotypic recognition sequences used for FLP-mediated neomycin and hygromycin cassette removal. The human *STXBP1* transgene is flanked with loxP sites. 5' regulatory region indicates promoter and proximal enhancers. (**B**) qPCR from gDNA of wild-type (+/+), hybrid (Hu/+) and fully humanized (Hu/Hu) *Stxbp1* model mice. *Tert* was used as endogenous control. (**C**) Kaplan-Meier survival curves of *Stxbp1*$^{Hu/+}$ and *Stxbp1*$^{Hu/Hu}$ mice. (**D**) Body weights of *Stxbp1* model mice. Red arrow indicates the last data available for male *Stxbp1*$^{Hu/Hu}$. (**E**) Genotypic ratios from the offspring of *Stxbp1*$^{Hu/+}$ x *Stxbp1*$^{Hu/+}$ breedings. Cartoon was created with BioRender. (**F**) RT-qPCR from cerebral cortex tissue of 8-week-old *Stxbp1* model mice. *Atp5f1* mRNA was used as endogenous control. (**G**) STXBP1 western blot from samples in (**F**). ATP5F1 was used as endogenous control. (**B**, **D**, **F** and **G**) Data are represented as mean values ± SEM. Data points represent independent biological replicates. (**F** and **G**) White and gray data points indicate females and males, respectively. (**B, F** and **G**) One-way ANOVA with Dunnett's multiple comparison test vs. wild-type (+/+). (**C**) Mantel-Cox test. (**D**) 2-way ANOVA with Dunnett's multiple comparison test vs. wild-type (+/+). (**E**) Chi-square test (df = 2, n = 161). FC, fold change. ns, non-statistically significant.

Figure 3. Molecular characterization of a *Syngap1* humanized-haploinsufficient mouse model. (**A**) Cartoon depicting the breeding scheme utilized to generate the *Syngap1* humanized-haploinsufficient mouse model and the corresponding genotypic ratios from the offspring. Created with BioRender. (**B**) Body weights of *Syngap1* humanized-disease mice. (**C**) RT-qPCR from hemi-brain tissue of 34-week-old and 14 to 23-week-old *Syngap1* humanized-haploinsufficient and *Syngap1* heterozygous haploinsufficient mice, respectively. *Actb* and *Atp5f1* mRNA were used as endogenous control. (**D**) SYNGAP1 western blot from samples in (**C**). ATP5F1 was used as endogenous control. (**E**) Phosphorylated ERK and total ERK western blots from samples in (**C**). (**B**, **C**, **D** and **E**) Data are represented as mean values ± SEM. Data points represent independent biological replicates. (**C**, **D**, **E**) White and gray data points indicate females and males, respectively. (**A**) Binomial test. (**B**) 2-way ANOVA with Sidak's multiple comparison test (**C**, **D** and **E**) Unpaired t-test. FC, fold change. ns, non-statistically significant.

Figure 4. Phenotypic characterization of the *Syngap1* humanized-haploinsufficient mouse model. Open field testing of 4 and 30 week old mice for (**A**) overall activity levels via total distance traveled, (**B**) number of stereotypic behaviors and (**C**) total time in center of arena. (**D**) Elevated plus maze testing for time in open arms and (**E**) number of open arm entries. (**F**) Horizonal ladder testing from 4 and 30 week old mice for number foot slips per 5 trials. (**G**) Learning phase of Barnes maze testing from 4 and 30 week old mice. (**H**) Barnes maze test day, time to target hole contact. (**A, B, C, D, E, F**, and **H**) Data are represented as mean ± SD. Dots represent individual animals, white and gray data points indicate females and males, respectively. (**G**) Data are represented by group means ± SD. (**A, C**, and **D**) Unpaired t-test (**B, E, F**, and **H**) Mann-Whitney (**G**) 2-Way repeated measures ANOVA (5 weeks genotype P = 0.51, 31 weeks genotype P = 0.14)

Figure 5. Bidirectional modulation of human *SYNGAP1* expression in *Syngap1*$^{Hu/-}$-derived primary neurons using ASOs. (**A**) Cartoon schematic representing the ASO-mediated splice-switching approach to upregulate human *SYNGAP1* expression by disrupting PTBP binding to *SYNGAP1* pre-mRNA. (**B**) Left, cartoon depicting the breeding scheme used to obtain *Syngap1*$^{Hu/-}$ embryos for primary neuron isolation. Created with Biorender. Right, RT-qPCR from *Syngap1*$^{Hu/-}$ primary cortical neurons treated with ASOs for 7 days. All ASOs were added at 10 µM except for Gap-SYN, which was added at 3 µM. ET-SC2 was used as a non-targeting ASO control. (**C**) RT-qPCR from *Syngap1*$^{Hu/-}$ primary cortical neurons treated with ASOs for 7 days. *Atp5f1* mRNA was used as endogenous control. A qPCR assay spanning exons 16-17 of human *SYNGAP1* was used. *Atp5f1* mRNA was used as endogenous control. (**B**) One-way ANOVA with Dunnett's multiple comparison test vs. mock-treated cells (-). (**C**) Kruskal-Wallis with Dunn's multiple comparison test vs. mock-treated cells. Data are represented as mean values ± SEM. Data points represent independent biological replicates. Alt. 3'ss, alternative 3' splice site. FC, fold change.

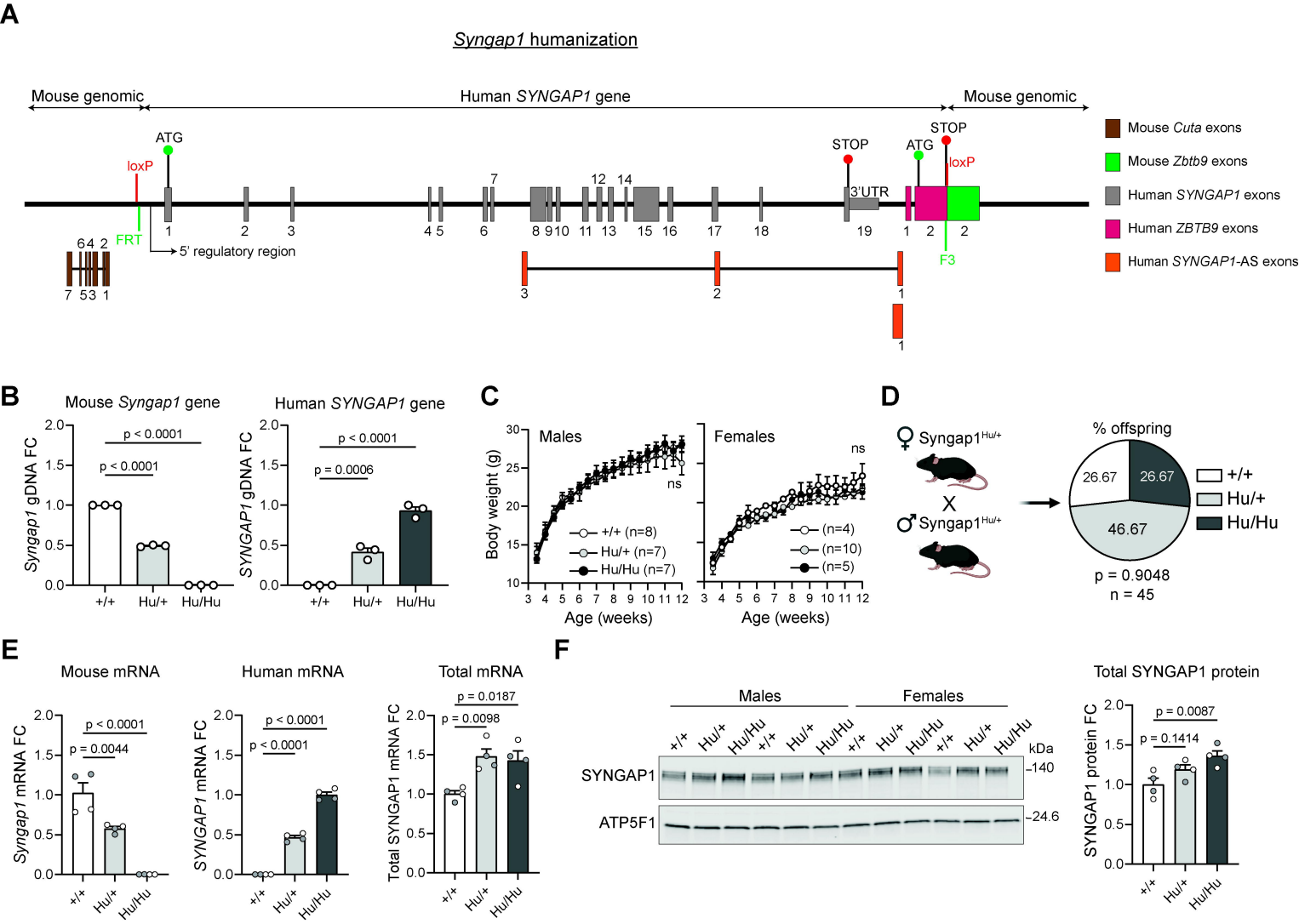
A
Syngap1 humanization
Mouse genomic
Human SYNGAP1 gene
Mouse genomic
ATG
loxP
FRT
5' regulatory region
STOP
3'UTR
ATG
STOP
loxP
F3
Mouse Cuta exons
Mouse Zbtb9 exons
Human SYNGAP1 exons
Human ZBTB9 exons
Human SYNGAP1-AS exons
B
Mouse Syngap1 gene
Syngap1 gDNA FC
p < 0.0001
p < 0.0001
+/+
Hu/+
Hu/Hu
Human SYNGAP1 gene
SYNGAP1 gDNA FC
p < 0.0001
p = 0.0006
C
Males
Females
Body weight (g)
Age (weeks)
+/+ (n=8)
Hu/+ (n=7)
Hu/Hu (n=7)
(n=4)
(n=10)
(n=5)
ns
D
Syngap1Hu/+
Syngap1Hu/+
% offspring
26.67
26.67
46.67
+/+
Hu/+
Hu/Hu
p = 0.9048
n = 45
E
Mouse mRNA
Syngap1 mRNA FC
p < 0.0001
p = 0.0044
Human mRNA
SYNGAP1 mRNA FC
p < 0.0001
p < 0.0001
Total mRNA
Total SYNGAP1 mRNA FC
p = 0.0187
p = 0.0098
F
Males
Females
SYNGAP1
ATP5F1
kDa
140
24.6
Total SYNGAP1 protein
SYNGAP1 protein FC
p = 0.0087
p = 0.1414

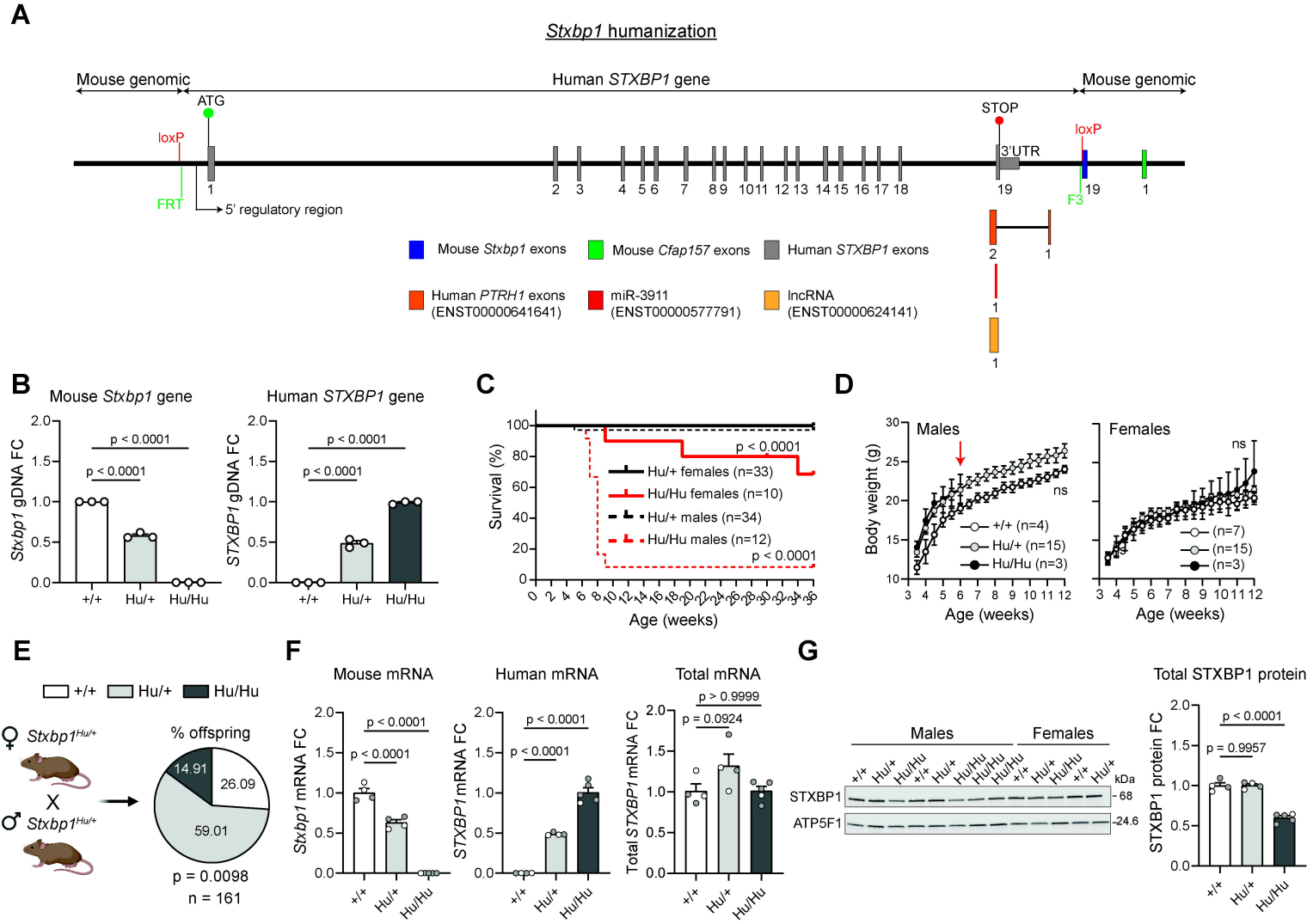
A
Stxbp1 humanization
Mouse genomic
Human STXBP1 gene
Mouse genomic
ATG
STOP
loxP
3'UTR
loxP
FRT
5' regulatory region
F3
Mouse Stxbp1 exons
Mouse Cfap157 exons
Human STXBP1 exons
Human PTRH1 exons (ENST00000641641)
miR-3911 (ENST00000577791)
lncRNA (ENST00000624141)
B
Mouse Stxbp1 gene
Human STXBP1 gene
Stxbp1 gDNA FC
STXBP1 gDNA FC
p < 0.0001
+/+
Hu/+
Hu/Hu
C
Survival (%)
Hu/+ females (n=33)
Hu/Hu females (n=10)
Hu/+ males (n=34)
Hu/Hu males (n=12)
Age (weeks)
D
Males
Females
Body weight (g)
+/+ (n=4)
Hu/+ (n=15)
Hu/Hu (n=3)
ns
Age (weeks)
E
+/+
Hu/+
Hu/Hu
Stxbp1Hu/+
X
Stxbp1Hu/+
% offspring
14.91
26.09
59.01
p = 0.0098
n = 161
F
Mouse mRNA
Human mRNA
Total mRNA
Stxbp1 mRNA FC
STXBP1 mRNA FC
Total STXBP1 mRNA FC
p < 0.0001
p > 0.9999
p = 0.0924
G
Males
Females
STXBP1
ATP5F1
kDa
68
24.6
Total STXBP1 protein
STXBP1 protein FC
p = 0.9957

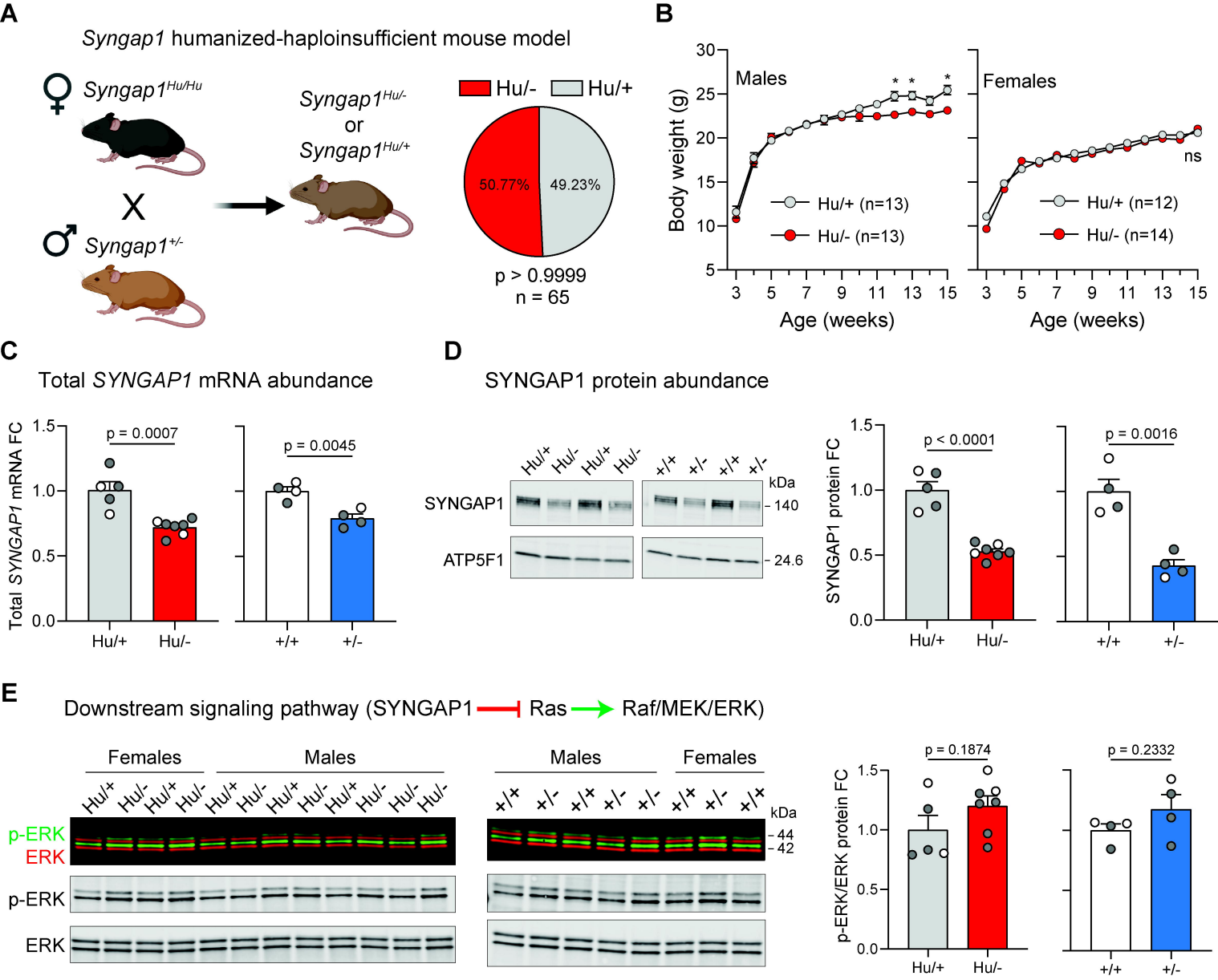
A
Syngap1 humanized-haploinsufficient mouse model
♀ Syngap1Hu/Hu
X
♂ Syngap1+/-
Syngap1Hu/-
or
Syngap1Hu/+
Hu/-
Hu/+
50.77%
49.23%
p > 0.9999
n = 65
B
Males
Females
Body weight (g)
Hu/+ (n=13)
Hu/- (n=13)
Hu/+ (n=12)
Hu/- (n=14)
ns
Age (weeks)
C
Total SYNGAP1 mRNA abundance
Total SYNGAP1 mRNA FC
p = 0.0007
p = 0.0045
Hu/+
Hu/-
+/+
+/-
D
SYNGAP1 protein abundance
SYNGAP1
ATP5F1
kDa
140
24.6
SYNGAP1 protein FC
p < 0.0001
p = 0.0016
E
Downstream signaling pathway (SYNGAP1 ⊣ Ras → Raf/MEK/ERK)
Females
Males
p-ERK
ERK
44
42
p-ERK/ERK protein FC
p = 0.1874
p = 0.2332

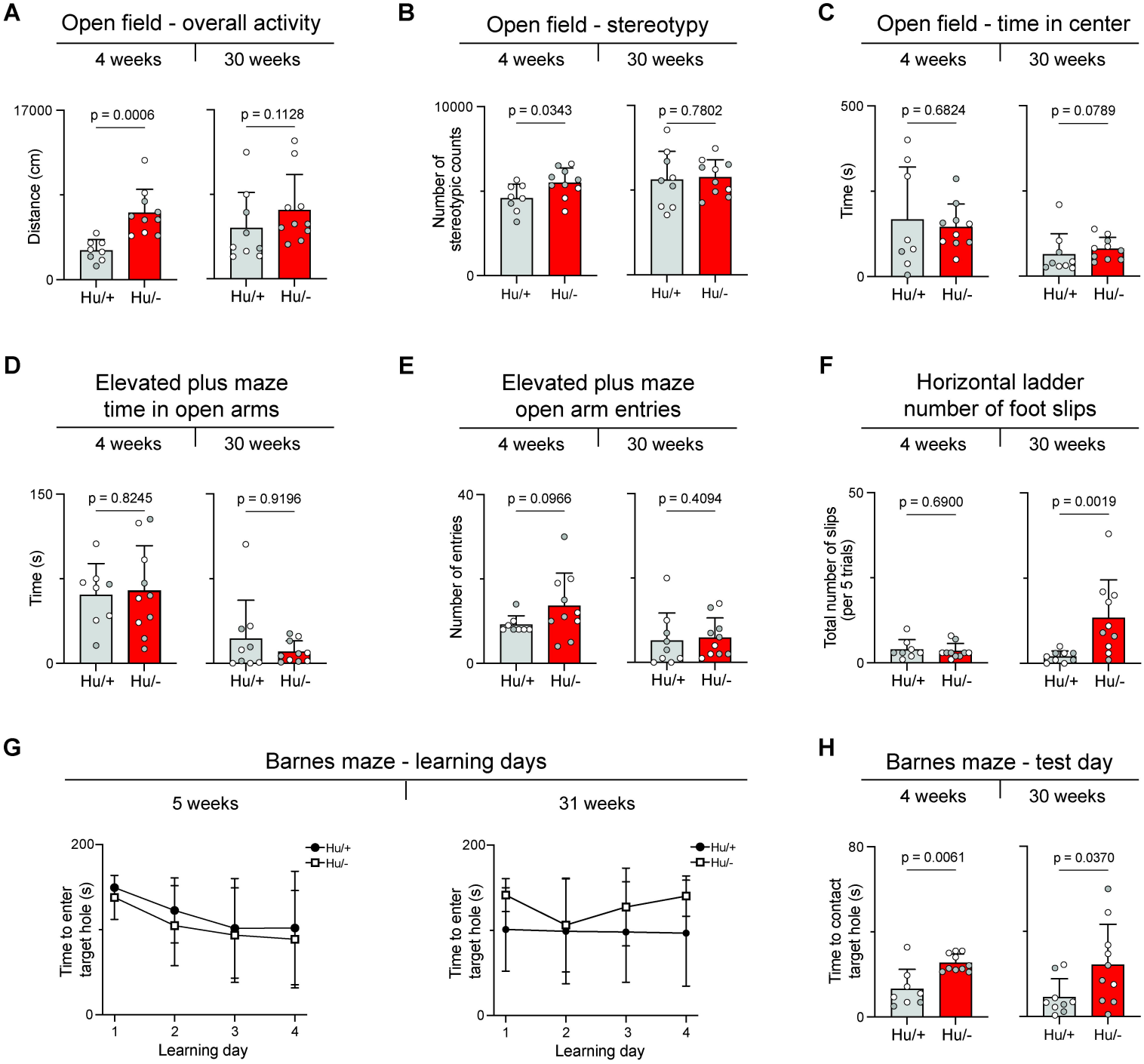
A
Open field - overall activity
4 weeks
30 weeks
17000
0
Distance (cm)
p = 0.0006
p = 0.1128
Hu/+
Hu/-
B
Open field - stereotypy
4 weeks
30 weeks
10000
0
Number of stereotypic counts
p = 0.0343
p = 0.7802
C
Open field - time in center
500
0
Time (s)
p = 0.6824
p = 0.0789
D
Elevated plus maze time in open arms
150
0
Time (s)
p = 0.8245
p = 0.9196
E
Elevated plus maze open arm entries
40
0
Number of entries
p = 0.0966
p = 0.4094
F
Horizontal ladder number of foot slips
50
0
Total number of slips (per 5 trials)
p = 0.6900
p = 0.0019
G
Barnes maze - learning days
5 weeks
31 weeks
200
0
Time to enter target hole (s)
Hu/+
Hu/-
1
2
3
4
Learning day
H
Barnes maze - test day
80
0
Time to contact target hole (s)
p = 0.0061
p = 0.0370

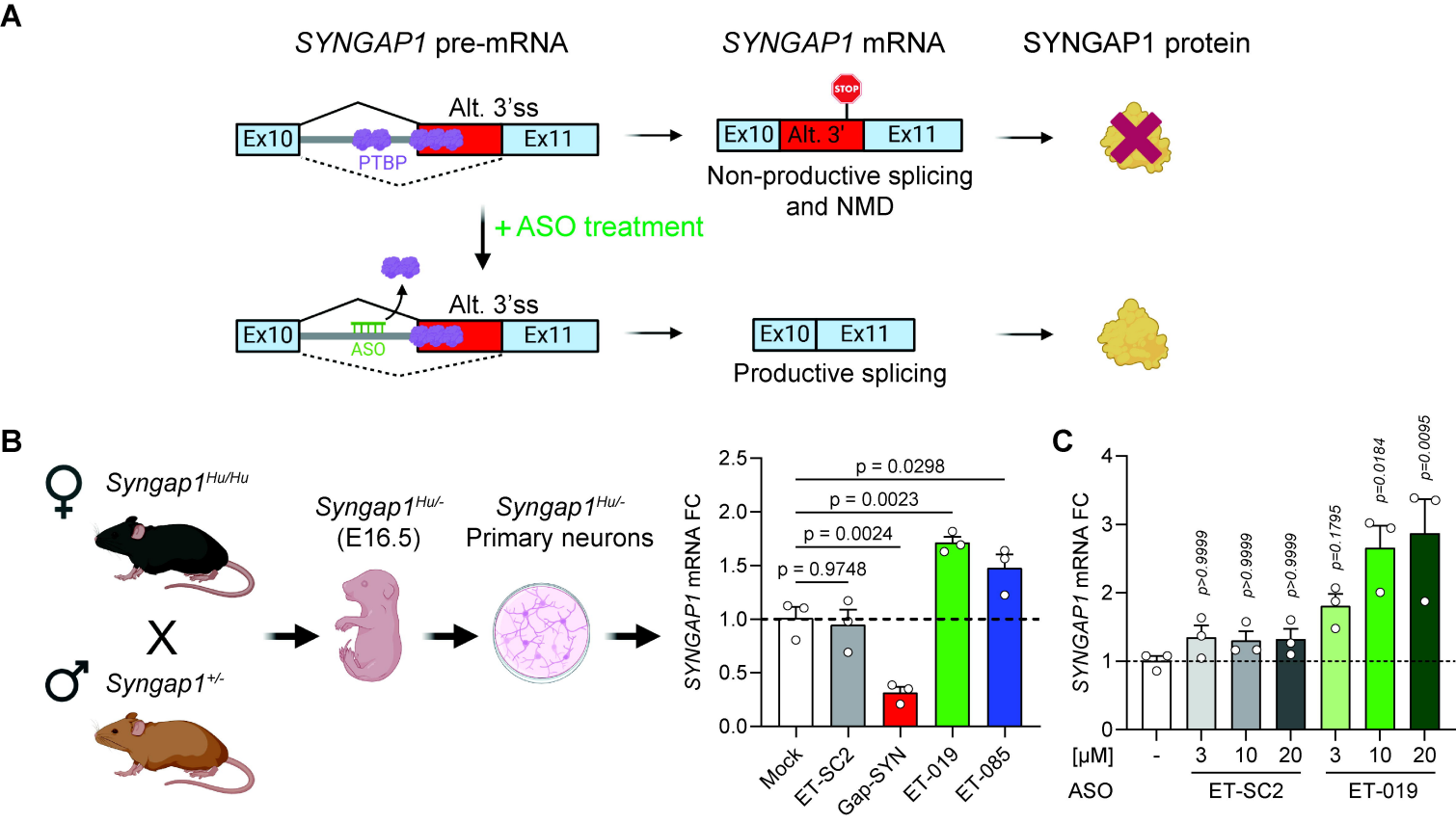
A
SYNGAP1 pre-mRNA
SYNGAP1 mRNA
SYNGAP1 protein
Alt. 3'ss
Ex10
Ex11
PTBP
STOP
Alt. 3'
Non-productive splicing and NMD
+ ASO treatment
ASO
Productive splicing
B
Syngap1Hu/Hu
Syngap1+/-
Syngap1Hu/-
(E16.5)
Syngap1Hu/-
Primary neurons
SYNGAP1 mRNA FC
p = 0.0298
p = 0.0023
p = 0.0024
p = 0.9748
Mock
ET-SC2
Gap-SYN
ET-019
ET-085
C
p<0.9999
p>0.9999
p<0.9999
p=0.1795
p=0.0184
p=0.0095
[μM]
ASO
ET-SC2
ET-019